Kim, H.W. and Duraisamy, K. and Brown, R.E. (2009) Effect of rotor stiffness and lift offset on the aeroacoustics of a coaxial rotor in level flight. In: 65th American Helicopter Society Annual Forum, 27-29 May 2009, Texas, USA.

http://strathprints.strath.ac.uk/27493/

Strathprints is designed to allow users to access the research output of the University of Strathclyde. Copyright © and Moral Rights for the papers on this site are retained by the individual authors and/or other copyright owners. You may not engage in further distribution of the material for any profitmaking activities or any commercial gain. You may freely distribute both the url (http://strathprints.strath.ac.uk) and the content of this paper for research or study, educational, or not-for-profit purposes without prior permission or charge. You may freely distribute the url (http://strathprints.strath.ac.uk) of the Strathprints website.

Any correspondence concerning this service should be sent to The Strathprints Administrator: eprints@cis.strath.ac.uk

Effect of Rotor Stiffness and Lift Offset on the Aeroacoustics of a Coaxial Rotor in Level Flight

Hyo Won Kim*
Postdoctoral Research Assistant

Karthikeyan Duraisamy
Lecturer in CFD

Richard E. Brown
Mechan Chair of Engineering

Rotorcraft Aeromechanics Laboratory
Department of Aerospace Engineering
University of Glasgow
Glasgow G12 8QQ
United Kingdom

Abstract

The acoustic characteristics of a twin contra-rotating coaxial rotor configuration with significant flapwise stiffness are investigated in steady forward flight. The Vorticity Transport Model is used to simulate the aerodynamics of the rotor system and the acoustic field is determined using the Ffowcs Williams-Hawkings equation implemented using the Farassat-1A formulation. Increasing the hub stiffness alters the strengths of the blade vortex interactions, particularly those between the upper and lower rotors, and affects the intensity and directivity of the blade vortex interaction noise produced by the system. The inter-rotor blade vortex interaction on the advancing side of the lower rotor is the principal source of the most intensively focused noise that is generated by a conventionally articulated coaxial rotor system. For stiffened coaxial rotors, this particular inter-rotor blade vortex interaction is weakened as a result of a broad redistribution in lateral loading, yielding a reduction in the intensity of the noise that is produced by this interaction. The spanwise distribution of loading on the rotors of a stiffened coaxial system can be modified further by altering the lateral partition of lift (or lift offset). It is shown that decreasing the lift offset has the effect of counteracting the redistribution of loading due to flapwise stiffness and hence increases the blade vortex interaction noise as well as the power consumed by the rotor. Conversely, a reduction in both the power consumption and the blade vortex interaction noise is observed if the lift offset is increased, with the maximum benefit of lift offset being achieved at high speed. The computational results suggest that the noise from the dominant inter-rotor blade vortex interaction can be ameliorated through the use of lift offset control on stiffened coaxial systems, to the extent that the noise produced by this interaction can be made to be comparable to that produced by the other, weaker interactions between the two rotors of the system.

Nomenclature

Symbols:

C_{Mx}	rotor rolling moment coefficient
C_P	rotor power coefficient
C_T	rotor thrust coefficient
M_{tip}	tip Mach number
N_{bt}	total number of blades
R	rotor radius
t	observer time
y_{LOS}	lateral lift offset
Γ	circulation
μ	advance ratio
ν	non-dimensional first harmonic flapping frequency
Ω	rotor rotational frequency
ψ	blade azimuth

Abbreviations:

BVI	blade vortex interaction
LOS	lift offset
VTM	Vorticity Transport Model
SPL	sound pressure level (dB)
OASPL	overall SPL (dB)
BVISPL	blade vortex interaction SPL (mid frequency 5–40/rev) (dB)

* Corresponding author; e-mail: hkim@aero.gla.ac.uk

Presented at the American Helicopter Society 65th Annual Forum, Grapevine, TX, 27–29 May 2009. Copyright © 2009 by the American Helicopter Society International, Inc. All rights reserved.

Note: throughout this paper, the lower rotor of the coaxial system should be taken to rotate anticlockwise, and the upper rotor to rotate clockwise, when viewed from above.

Introduction

Modern requirements for helicopters with increased speed and load-carrying capabilities have prompted several novel configurations to be explored. One such approach, put forward by Sikorsky Aircraft Corporation and called the 'X2' concept, is a thrust-compounded, rigid coaxial helicopter. The main rotor system of the X2 technology demonstrator consists of a twin contra-rotating coaxial rotor that is very stiff in both flap and lag [1]. A similar technology, though different in its detailed design, was employed in the Advancing Blade Concept (ABC) rotor of the Sikorsky XH-59A [2]. The advantage of a stiff coaxial system over a conventionally articulated system is that, at high forward speeds, most of the lift can be carried on the advancing sides of the rotors where the dynamic pressure is high. Consequently, the high lift coefficients associated with the retreating side of conventionally articulated rotors can be alleviated within the stiffened rotor system, with consequent benefits for the power consumption of the rotor. Since the twin rotors counter-rotate, the aerodynamic rolling moment that results from any lateral imbalance in the distribution of lift on one of the rotors can be counteracted by the production of an equal and opposite rolling moment by the other rotor of the system [3–5].

In a previous study [6], the conventionally articulated coaxial rotor was shown to consume less power than the equivalent conventional single rotor. This reduction was shown to be mainly due to a reduction in the induced component of power that is consumed by the coaxial rotor compared to the equivalent single rotor. Furthermore, increasing the flapwise stiffness of a coaxial system has been shown to reduce its induced power consumption further [7]. There is an added advantage for a coaxial configuration over a conventional main rotor – tail rotor configuration in that the need for the tail rotor is eliminated. This is because the required torque balance is achieved inherently within the contra-rotating main rotor system. It should be borne in mind, however, that the additional power consumed by the tail rotor in a single rotor platform decreases notably as the forward speed is increased [8], and also that the drag penalty associated with the enlarged rotor mast of the coaxial rotor, particularly for the conventionally articulated system, increases with speed [9].

In terms of acoustic performance, previous studies have suggested that a coaxial rotor generates higher sound pressure levels than an equivalent single rotor in level flight [10–12]. This is perhaps unsurprising since coaxial rotors have an additional source of noise, compared to single rotor systems, that results from the interaction between the wake of the upper rotor and blades of the lower rotor of the system. Indeed, for the articulated coaxial rotor, the most intense impulsive noise is generated by inter-rotor blade vortex interactions (BVIs) on the advancing side of the lower rotor [12]. The noise associated with these BVIs has been shown to intensify with increasing flight speed due to the increasing strength of the interaction between the wake of the upper rotor and the blades of the lower rotor.

Many of the aerodynamic and aeroacoustic attributes that are unique to a stiff coaxial system arise from the manner in which the load is distributed over the rotor discs. The load distribution on a stiff coaxial system is fundamentally different to that on a conventionally articulated system in that the loading on the stiff coaxial system is heavily biased towards the advancing sides of its rotors. As a result, the effective lift vector need not act through the centre of each rotor of the stiff coaxial system. The lift offset[1] (LOS), can be controlled by applying differential cyclic pitch between the upper and the lower rotors [1, 2], and the associated redistribution in loading can be exploited to improve the performance of the rotor [1]. While it was initially believed that the power consumption and stability characteristics of the XH-59A were largely insensitive to any variation in the lift offset [2], it was later shown that the efficiency of the X2 rotor could indeed be optimised using lift offset control [1]. Improvements in the performance of the X2 rotor at high forward speed, as predicted using Sikorsky's design software and reported by Bagai [1], should result from increasing the lift offset and redistributing the loading towards the region of higher incident velocity on the advancing sides of its rotors.

The ability to modify the loading distribution on the rotor by controlling the lift offset offers the possibility of altering the character of the inter-rotor interaction which is known to be the principal source of noise within the coaxial rotor configuration. Despite increasing interest in the performance of coaxial rotor systems, detailed aeroacoustic analyses, particularly for stiff coaxial systems, are rarely found in the open literature. The aim of this paper is to lend insight into the acoustic characteristics of a stiff coaxial rotor in forward flight, with specific focus on the effect of flapwise stiffness on the contribution that is made by the blade vortex interactions within the system to the acoustic signature of the rotor. In addition, the sensitivity of the acoustic signature of the coaxial rotor to changes in its lift offset is investigated.

[1] Lift offset is defined as the lateral distance between the centre of rotation of the rotor and the point through which integrated effective lift of the rotor acts.

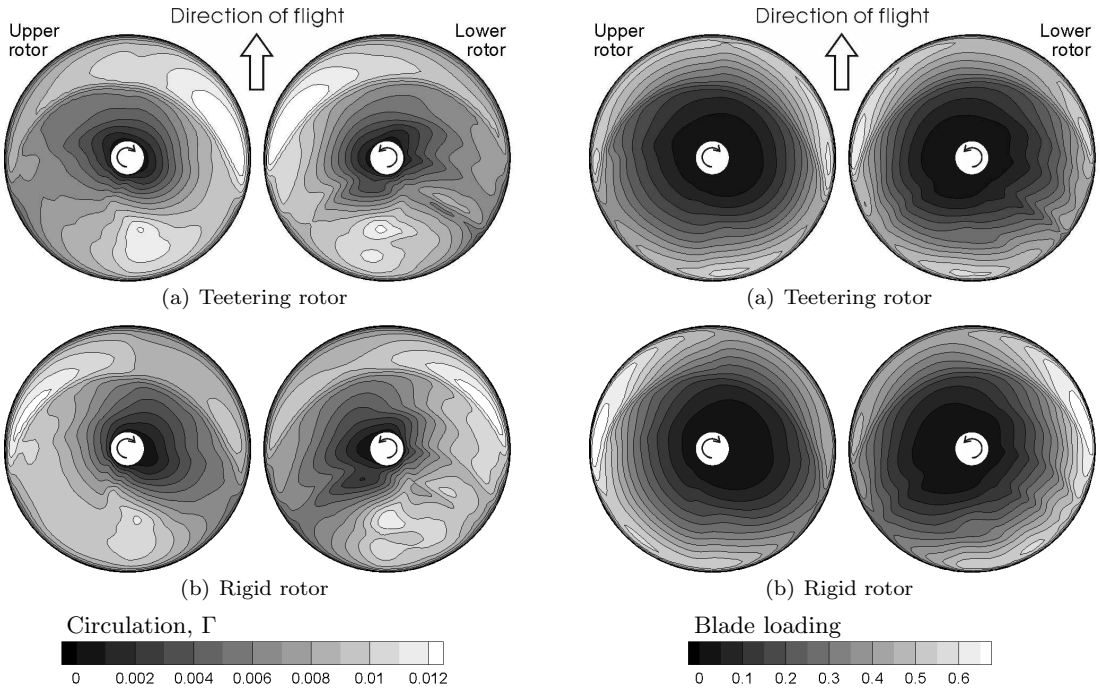

Figure 1: *Distributions of circulation and blade loading on upper and lower rotors of the coaxial system at advance ratio* $\mu = 0.12$ *and thrust coefficient* $C_T = 0.0048$. *Teetering and rigid rotors compared.*

Computational Model

The Vorticity Transport Model (VTM) developed by Brown [13, 14] has been used to simulate the aerodynamics of the coaxial rotor. In the VTM, the aerodynamics of the rotor blades are modelled using an extension of the Weissinger-L formulation of lifting-line theory in conjunction with look-up tables for the sectional aerodynamic characteristics of the blade sections. The equations of motion of the blades, as forced by the aerodynamic loading along their span, are derived by numerical differentiation of a pre-specified non-linear Lagrangian for the modelled system. The VTM uses an Eulerian representation of the vorticity in the rotor wake, which is advanced through time by solving the incompressible Navier Stokes equations in vorticity-velocity form on a structured grid surrounding the rotor. The problem of numerical diffusion of vorticity that is endemic to more conventional CFD techniques is avoided by explicitly conserving the vorticity within the flow by using this approach. The vorticity transport equation is solved using a finite volume TVD-type scheme which allows the integrity of the vortical structures in the wake to be preserved for long times. The VTM is thus ideally suited to resolving the detailed features of the interactions between the upper and lower rotors of the coaxial system that are known to be significant sources of noise [7, 12].

The acoustic field generated by the rotor system is determined using the Farassat-1A formulation of the Ffowcs Williams-Hawkings equations [15]. Since the blade surface is represented by a series of panels along the length of the blade, the force contributed by each panel is treated as a point acoustic source at the panel collocation point. The instantaneous acoustic pressure at any given observer location is then given by the sum of the contributions from all the point sources that are present in the computational domain. Since the lifting-line model assumes an infinitesimally thin blade, the thickness noise is modelled independently using a source-sink pair attached to each collocation point [16]. Noise due to quadrupole sources is neglected in the present work. The coupled VTM-acoustics methodology has been used previously to predict the acoustics of the HART II rotor [17], where good agreement between the computed pressure time histories and sound pressure levels was demonstrated against measured data for three representative flight conditions involving strong BVIs [18].

Rotor Configuration

The rotor configuration used in this study mimics that used by Harrington (referred to as 'rotor 1' in Ref. 19), which consisted of identical, twin, two-bladed contra-rotating rotors with a teetering hub. Flapwise stiffness in the system is modelled by applying a spring across each of the flapping hinges of the rotor independently. The stiffness of the

Table 1: *Summary of rotor dimensions*

Rotor radius	3.81 m
Rotor speed	37.52 rad/s
Tip Mach number	0.42

springs is chosen to give the desired natural flapping frequency of the rotor blades. To match the flight conditions of the original experiments conducted by Dingeldein [20], where the power consumption of Harrington's rotor was measured in steady forward flight, the tip Mach number, M_{tip}, was set to 0.42. As in the experiment, the rotor was simulated at a constant thrust coefficient $C_T = 0.0048$, and, in all cases, the system was trimmed to zero overall yawing moment using differential collective pitch input. In all simulated cases, coupled longitudinal cyclic control inputs to the individual rotors of the coaxial system were used to tilt the thrust vector forward in order to represent the propulsive force required to overcome the drag of a fuselage with a flat-plate area of 0.02 times the rotor area (as was done in Dingeldein's experiment).

Two different methods of applying the lateral cyclic pitch input required to trim the coaxial rotors were implemented. In the first method, the cyclic pitch inputs to the upper and lower rotor are coupled such that both rotors receive the same control inputs. The coupled cyclic input is then used to achieve overall zero lateral force and moment on the system. The second method uses independent (differential) cyclic pitch inputs to the individual rotors of the coaxial system and is applied exclusively to the coaxial rotors with non-zero flapwise stiffness. This method allows the lateral lift offset on the rotors to be controlled whilst still maintaining zero overall rolling moment on the system.

In all the analyses presented in this paper, the acoustic sources are scaled to represent the noise that was generated by the specific rotor that was used by Harrington and Dingeldein in their experiments. The dimensions and relevant operating conditions of this rotor are summarised in Table 1.

Effect of Rotor Stiffness on Acoustic Characteristics

The effect of hub stiffness on the acoustic characteristics of the coaxial rotor is investigated by comparing the behaviour of the teetering configuration to that of two other rotor systems that are geometrically identical but have different flapwise stiffnesses. The first case to be considered is that of the stiffened system with a flap spring selected to give a natural frequency of the first flapping mode of 1.5Ω. The second case to be considered is that of the completely rigid system with infinite flapwise stiffness. The rotor blades themselves are assumed to be rigid in order to simplify the comparison between the various cases that are presented. By this artifice, any obscuration of the fundamental aerodynamics that underpin the acoustic behaviour of the system that might arise, for instance, from the details of mode shapes, is avoided. Furthermore, the chosen values of stiffness have been shown previously to yield reasonable approximations [7] to the dynamic behaviour of representative full-scale systems such as the XH-59A [4, 5]. In order to expose the effects of hub stiffness, the acoustic characteristics of these stiffened systems are compared to those of the original teetering configuration as used in Dingeldein's experiments. Detailed analysis of the acoustic properties of the stiffened coaxial rotors in forward flight is limited however to two representative flight speeds (at advance ratios of $\mu = 0.12$ and 0.24) in order simply to contrast the differences in the behaviour of the systems at low and at high advance ratio.

Consequences for BVI Noise

It was shown in Ref. 7 that stiffening the hub of a coaxial system results in a broad redistribution of lift over the rotor discs (see Figure 1). The load on the stiffened system is redistributed laterally such that the advancing blades carry higher lift (and vice versa for the retreating blades) than when the hubs of the rotors are articulated. As a consequence, the strengths of the trailed tip vortices of the stiffened system are modified and this results in a subtly different wake structure to that of a conventionally articulated system. The change in the strength of the vortices is not severe enough to distort the wake to the extent that the positions of the BVIs on the rotor discs are affected significantly, however. This notion is supported by the comparison of the BVI patterns shown in Figure 2 for the rotors with different stiffnesses. In this figure, the positions of the BVI events in both low and high speed flight are seen to be largely independent of the flapwise stiffness of the hubs of the rotors. More importantly, though, the strengths of these BVIs, particularly of the inter-rotor BVIs on the advancing side of the lower rotor, can be seen to be modified (as indicated by the density of the contour lines) by changing the stiffness of the rotor. The change in strength of the BVIs is a direct consequence of the lateral redistribution of loading across the rotor disc that arises due to the introduction of hub stiffness.

The relative strength and intensity of these interactions has a profound effect on the acoustic signature of the rotor system. The strength of the acous-

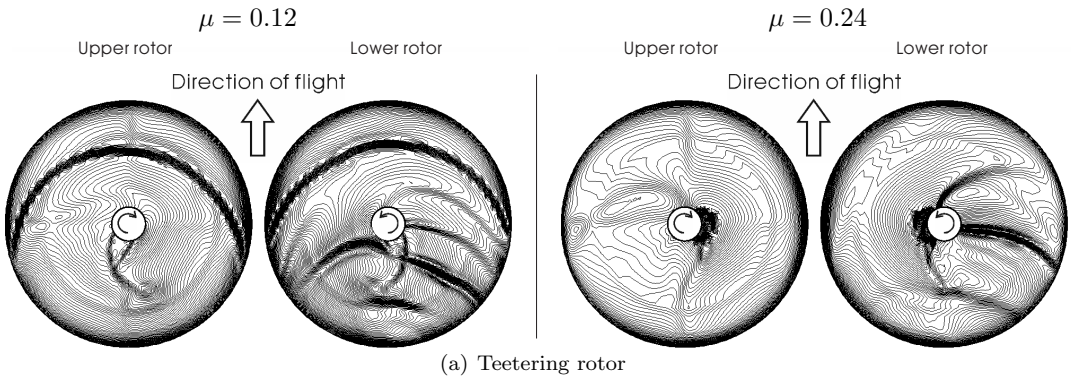

(a) Teetering rotor

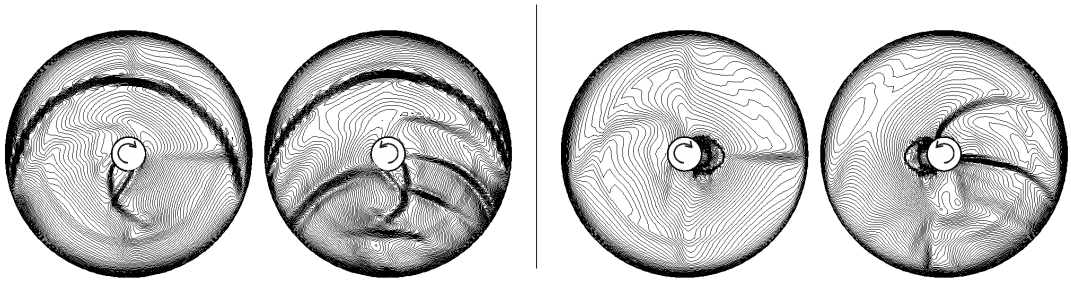

(b) Rotor stiffened to give first flapping frequency $\nu = 1.5$

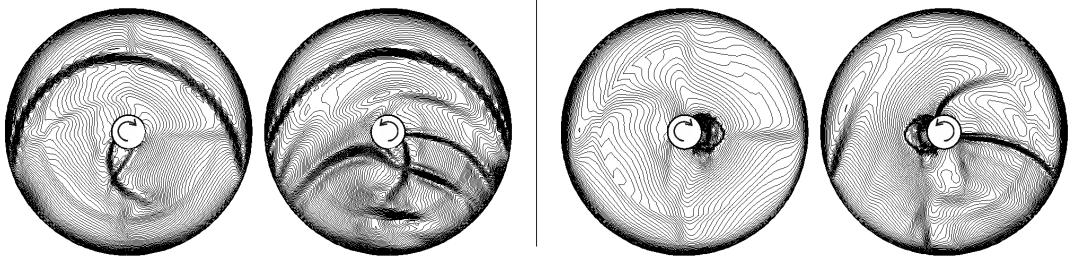

(c) Rigid rotor

Figure 2: *BVI patterns on the upper and lower rotors of the coaxial system, visualised using contours of inflow. Advance ratio* $\mu = 0.12$ *(left) and* $\mu = 0.24$ *(right).*

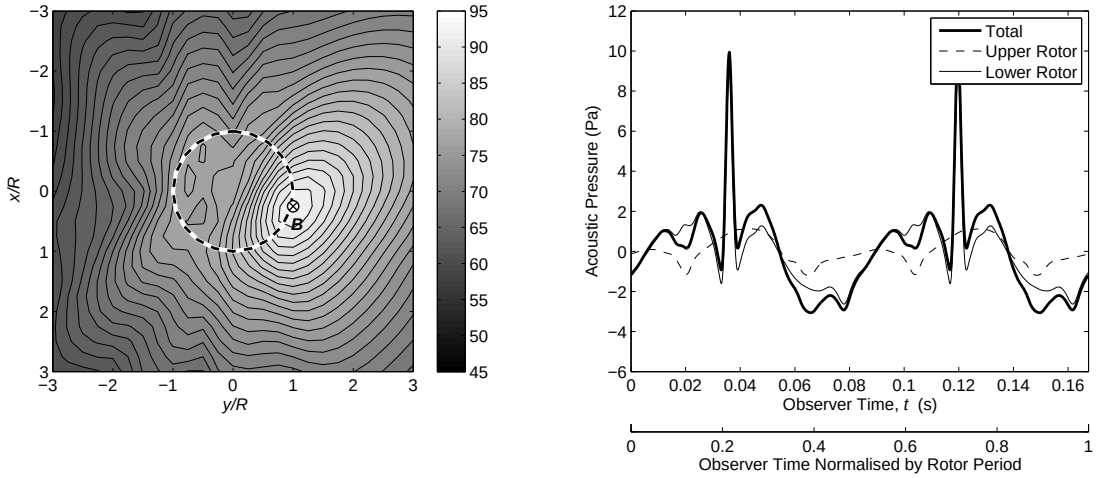

(a) Teetering rotor (sound pressure at 'B' is 92.3 dB)

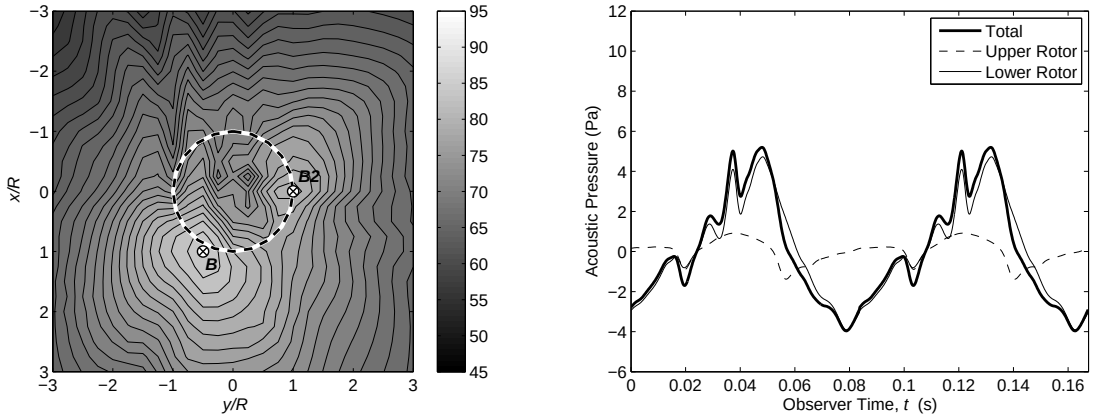

(b) Rotor stiffened to give first flapping frequency $\nu = 1.5$ (sound pressure at 'B2' is 80.9 dB)

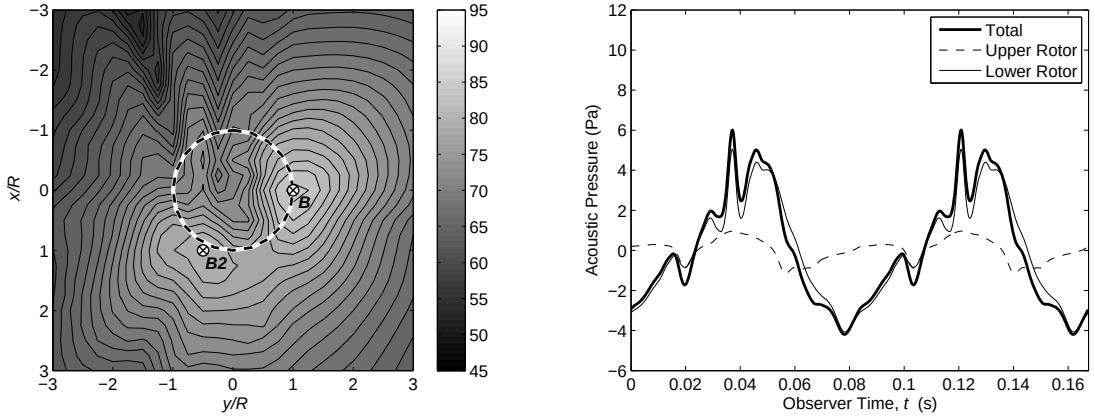

(c) Rigid rotor (sound pressure at 'B' is 84.3 dB)

Figure 3: *BVI sound pressure levels (5–40N_{bt}/rev) in decibels on a plane 1R below the hub of the lower rotor (left) and time history of acoustic pressure over one rotor revolution (right) at the BVI hot spot on the advancing side of the lower rotor. Advance ratio* $\mu = 0.12$.

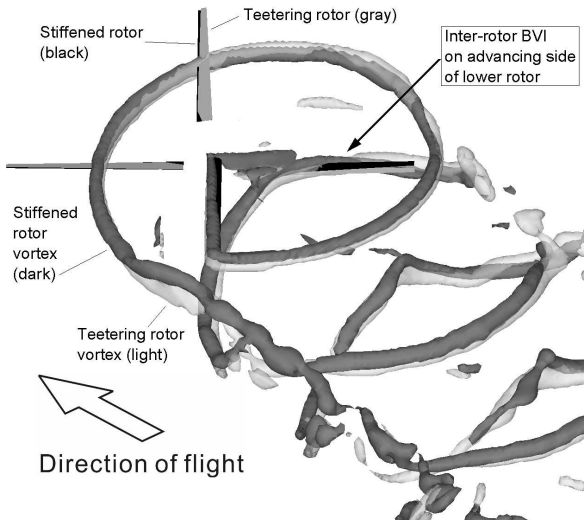

Figure 4: *Geometry of the principal inter-rotor BVI on the advancing side of the lower rotor. Teetering and stiffened rotors compared at advance ratio* $\mu = 0.12$.

tic radiation from the rotor is directly related to the time rate of change in blade loading, and hence the rapid changes in loading on the blades due to the blade vortex interactions shown in Figure 2 play an important role in determining the overall acoustic character of the coaxial rotor system.

Figure 3 compares the BVI sound pressure level that is observed on a horizontal plane, located $1R$ below the hub of the lower rotor, for the coaxial systems of various stiffnesses when operating at advance ratio $\mu = 0.12$. Also shown in Figure 3 is the time history of the acoustic pressure at the localised peaks (acoustic hot spots) on the observer plane as indicated in the diagrams to the left of the figure. It should be noted that, for both the stiffened and the rigid coaxial rotors, the distribution of acoustic sound pressure on the plane below the rotor contains two localised peaks in the observer plane. One peak is directly below the advancing side of the lower rotor and the other is below the rear of the disc. Interestingly, the hot spots below the advancing side of the lower rotor of the stiffened and the rigid rotors coincide with the only distinct peak in the acoustic signature of the articulated coaxial rotor, suggesting a common aerodynamic origin for this feature.

Close examination of the time histories of acoustic pressure at the hot spot below the advancing side of the lower rotor, as shown in Figure 3, reveals that the acoustic signal from both the stiffened and the rigid rotors have a peak that occurs at an observer time $t = 0.036\,\mathrm{s}$, albeit with much reduced amplitude and impulsiveness compared to a similar peak in the acoustic pressure that is generated by the teetering configuration at the same observer time. The highly impulsive peak in the acoustic signal generated by the teetering configuration was shown in Ref. 12 to be due to a parallel BVI on the advancing side of the lower rotor. It is clearly evident in Figure 4, which compares the geometry of this particular inter-rotor BVI for the teetering and stiffened configurations, that, at the time of its impingement, the interacting vortex is aligned with the blade along a large proportion of its span. The change in the strength of this BVI that results from a change in the stiffness of the rotor can be inferred from the density of the contour lines at an azimuthal location of approximately 45° in Figure 2. The effect on the acoustic signature of the rotor of the weakening of this BVI can be inferred from the distribution of acoustic sources on the lower rotors of both the stiffened and the rigid systems, as shown in Figure 5. This figure shows the source density of the noise due to blade loading (evaluated from the loading noise term in the Ffowcs Williams-Hawkings equation and scaled by the local panel area) in 'source time' i.e. at the time corresponding to the location of the blade when the sound was generated. The distribution of the source density defined in this way will of course differ for each observer location. The plot is thus generated from the perspective of an observer located at the BVI hot spot below the advancing side of the lower rotor. The region of concentrated source density at approximately 45° azimuth that is present for the teetering rotor is not visible in the distributions for the stiffened rotor and the rigid rotor. Instead, the region of high acoustic source density is shifted outboard towards the tip region of the advancing side. This is a result of the increased loading gradient in this region of the rotor disc compared to that of the teetering rotor (see Figure 1). These observations reveal that the focusing of the distributed acoustic pressure to form the sharp peaks in acoustic pressure at the hot spot below the advancing side of the lower rotor is a direct consequence of the impulsive nature of the parallel blade vortex interaction on the advancing side of the lower rotor.

The secondary hot spot that is located below the rear of the disc, again for both the stiffened and the rigid rotors (see Figure 3), originates from the BVI on the retreating side of the lower rotor. In contrast to the weakening of the vortex that is involved in the inter-rotor BVI on the advancing side of the lower rotor as the stiffness of the system is increased, the vortex that interacts with the retreating blade of the lower rotor is strengthened. This is because this vortex originates from the advancing blade of the upper rotor where the loading is concentrated as the rotor is stiffened. As this vortex passes the retreating blade of the lower rotor, it yields an intensified inter-rotor BVI compared to that generated within the teetering rotor system.

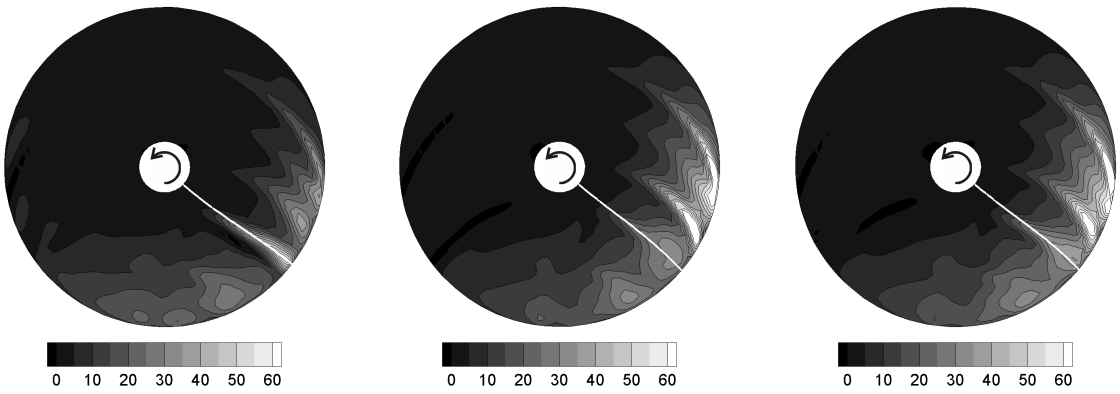

(a) Teetering rotor (b) Rotor stiffened to $\nu = 1.5$ (c) Rigid rotor

Figure 5: *Acoustic source density (loading noise, Pa/m^2) on the lower rotor of the coaxial system as evaluated at the BVI hot spot directly below the advancing side of lower rotor found at advance ratio $\mu = 0.12$. Also shown as a white line is the locus of sources corresponding to observer time $t = 0.037\,s$, in other words to the time when the acoustic peak is observed in Figure 3.*

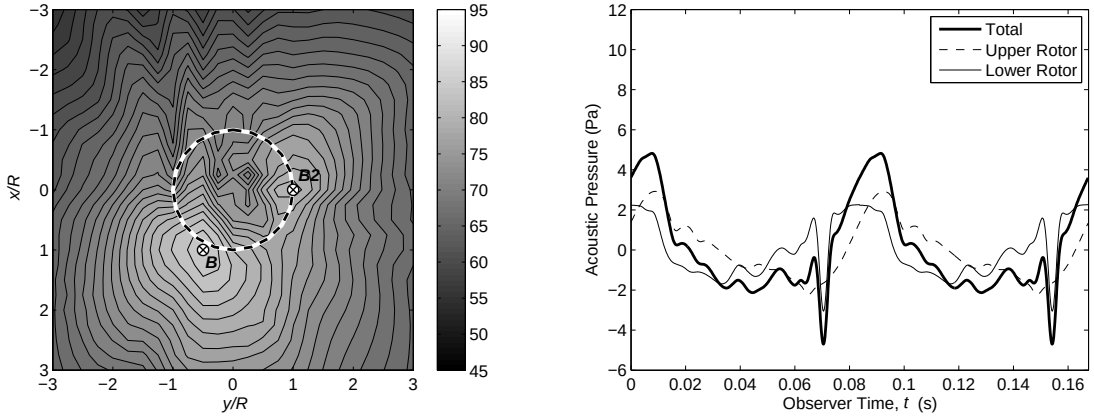

(a) Rotor stiffened to give first flapping frequency $\nu = 1.5$ (sound pressure at 'B' is 84.9 dB)

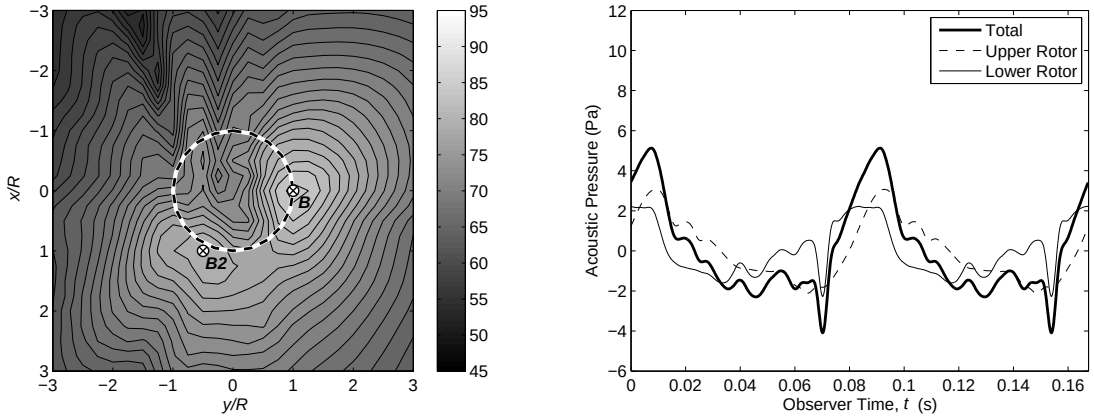

(b) Rigid rotor (sound pressure at 'B2' is 80.0 dB)

Figure 6: *BVI sound pressure levels (5–40N_{bt}/rev) in decibels on a plane $1R$ below the hub of the lower rotor (left) and time history of acoustic pressure over one rotor revolution (right) at the BVI hot spot below the rear of the rotor disc. Advance ratio $\mu = 0.12$.*

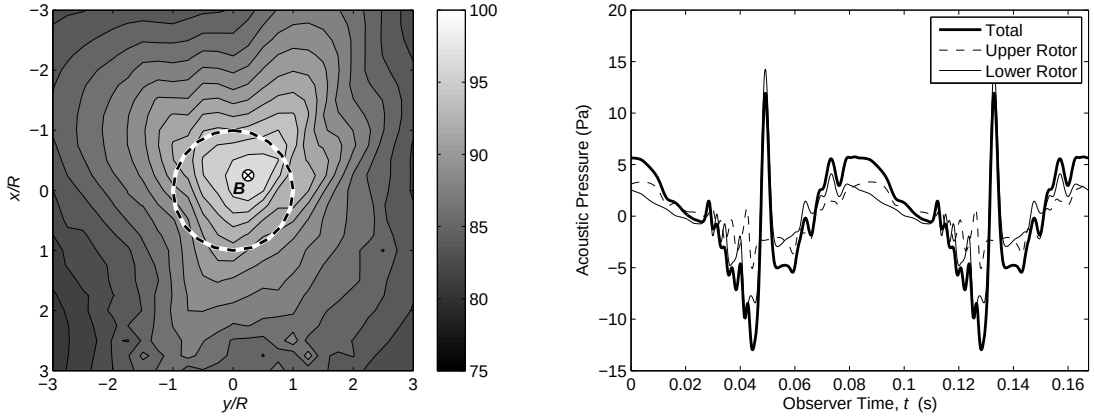

(a) Teetering rotor (sound pressure at 'B' is 97.4 dB)

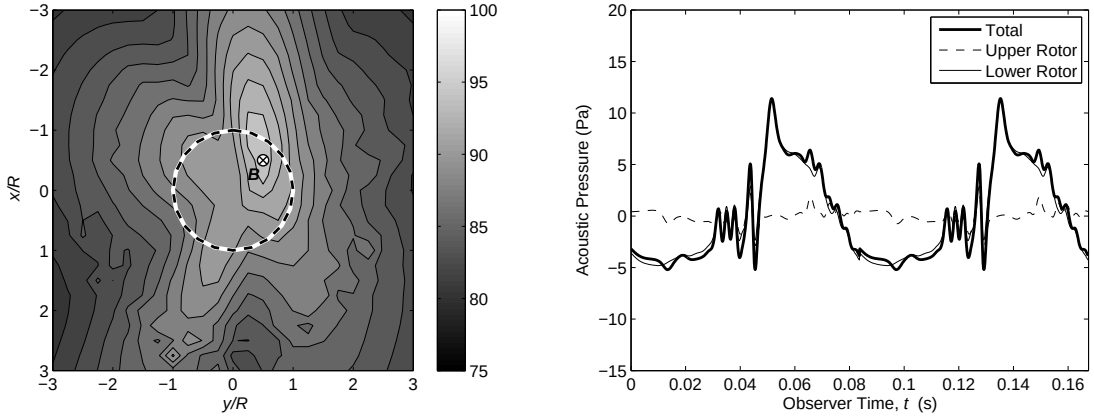

(b) Rotor stiffened to give first flapping frequency $\nu = 1.5$ (sound pressure at 'B' is 94.5 dB)

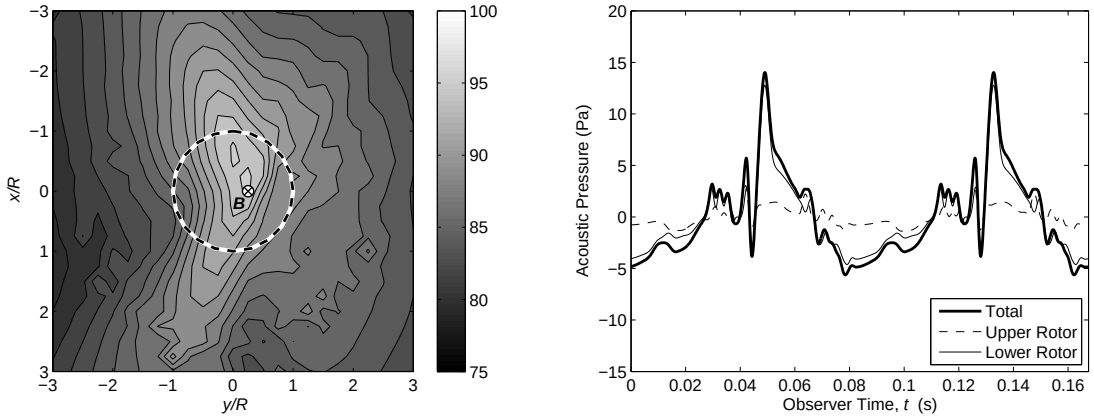

(c) Rigid rotor (sound pressure at 'B' is 95.4 dB)

Figure 7: *BVI sound pressure levels (5–40N_{bt}/rev) in decibels on a plane* $1R$ *below the hub of the lower rotor (left) and time history of acoustic pressure over one rotor revolution (right) at the BVI hot spot marked 'B'. Advance ratio* $\mu = 0.24$.

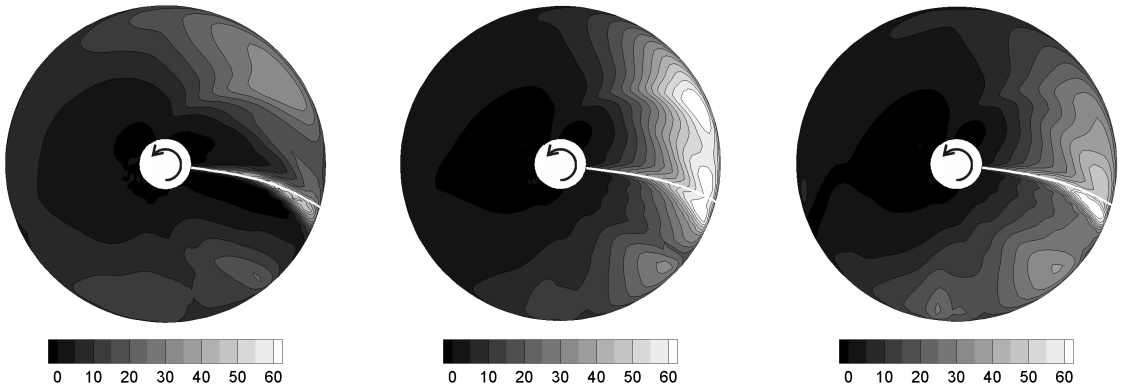

(a) Teetering rotor (b) Rotor stiffened to give $\nu = 1.5$ (c) Rigid rotor

Figure 8: *Acoustic source density (loading noise, Pa/m^2) on the lower rotor of the coaxial system as evaluated at the BVI hot spot found at advance ratio $\mu = 0.24$. Also shown as a white line is the locus of sources corresponding to observer time $t = 0.05$ s (and 0.134 s), in other words to the time when the acoustic peak is observed in Figure 7.*

The time histories of the acoustic pressure shown in Figure 6 reveals the peaks that are associated with this interaction to occur at an observer time of $t = 0.070$ s (and 0.154 s) and to culminate in the hot spot below the rear of the disc for both the stiffened rotor and the rigid rotor. It is also clear from this figure that the pressure pulse due to the inter-rotor BVI on the retreating side of the lower rotor is more impulsive in character for the stiffened rotor than it is for the rigid rotor.

It is interesting to note that the relative impulsiveness of the acoustic signature that is predicted for the stiffened and the rigid rotors is quite different, as is the maximum sound pressure level at the two hot spots below the rotor. Since an increase in the flapwise stiffness in the rotor system acts to bias the loading on the rotors towards the tips of their advancing sides, one might expect that the strengths of the inter-rotor BVIs would be most extreme in the limiting case of infinite stiffness. The rigid rotor should thus have the weakest acoustic radiation from the advancing side of the lower rotor and, similarly, the greatest amplification of noise below the retreating side of the lower rotor of the three systems that were examined. In that respect, the trends observed above may seem somewhat counter-intuitive. It should be borne in mind though that the strength of a BVI event, and thus the amplitude of the associated acoustic radiation, is not dependent solely on the strength of the vortex that interacts with the blade, but is also sensitive to subtle variations in the miss-distance and relative orientation of the interacting vortex with respect to the blade. Whilst the assumption of infinite stiffness yields a reasonable representation of the level of stiffness that is achievable in practical rotor systems, the results presented here indicate strongly that incorporation of the blade dynamics, including the structural deformation of the blades, is adviseable in any detailed study of a real helicopter system in order to capture accurately these secondary effects before any concrete conclusions regarding its acoustic performance are drawn.

It is evident from Figure 7 that, at high advance ratio ($\mu = 0.24$), the direction of propagation of the BVI noise is focused along the fore and aft axis of the coaxial system, particularly for the stiffened rotor and the rigid rotor. The source of this radiation is the parallel BVI that takes place when the blade is close to the point of maximum incident velocity (at $\psi = 90°$) on the advancing side of the lower rotor, and its longitudinal directivity is because, during a parallel vortex interaction, the radiation of sound is highly focused in the direction perpendicular to the blade [21, 22]. This particular interaction is responsible for the peaks in the acoustic pressure that occur at observer time $t = 0.05$ s, as shown in Figures 7 and 8. For the teetering configuration, this peak in acoustic pressure is highly impulsive in character. In the case of both the stiffened and the rigid systems, as shown in Figure 7, the impulsiveness of this particular inter-rotor BVI is ameliorated through the weakening of the interaction that results from the offloading of the retreating sides of the rotors. The reduction in BVI noise that is associated with an increase in hub stiffness, of about 2–3 dB as observed on the horizontal observer plane below the rotor, appears to be relatively limited compared to the reduction of 8 dB that is observed at low advance ratio ($\mu = 0.12$). It should be borne in mind though that the effect of thickness noise becomes significant at high speeds and hence may obscure the interpretation of the overall acoustic pattern of the system. The significance of the thickness component of the noise is discussed in more detail in the following section.

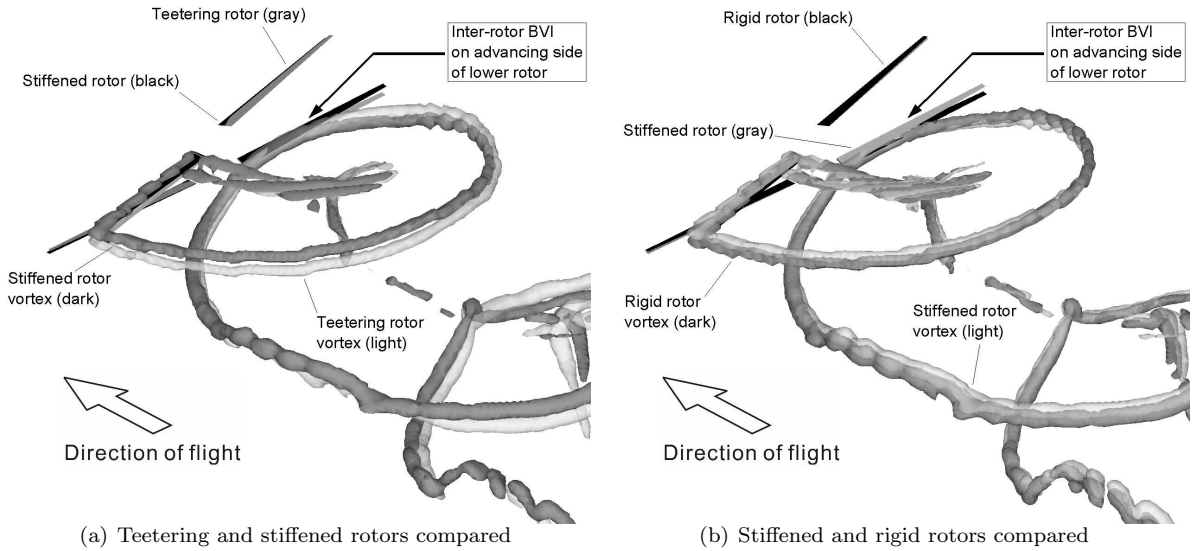

(a) Teetering and stiffened rotors compared

(b) Stiffened and rigid rotors compared

Figure 9: *Geometry of the principal inter-rotor BVI on the advancing side of the lower rotor. Advance ratio* $\mu = 0.24$.

The subtle differences in the exact location of the hot spots and in the direction of propagation of the BVI noise that is observed at high advance ratio for the various rotor systems can be attributed to differences in the relative orientation of the blades and the interacting vortices. These differences originate from the effect of flapwise stiffness in modifying the dynamic behaviour of the blades, notwithstanding the fact that the imposed trim conditions on the rotor system are identical in all cases. As a result, small differences in the orientation of the blade during this interaction yield subtle differences in the direction of noise propagation for the three different rotor systems. These smll geometric differences are revealed in Figure 9 which shows the influence of hub stiffness on the geometry of this particular inter-rotor BVI.

Consequences for Far-Field Noise

The characteristics of the far-field noise radiated by the rotor can be understood by considering the distribution of sound pressure on a hemispherical surface of radius $2R$, centred at the hub of the lower rotor of the coaxial system. To an observer in the far-field, this surface can be considered as a hemispherical source of sound with the same acoustic properties as the rotor system. Figures 10 and 11 show maps of the sound pressure level on this hemispherical surface that are generated by the rotors with the various hub stiffnesses at advance ratios of $\mu = 0.12$ and 0.24 respectively. At low forward speed ($\mu = 0.12$), the distribution of BVI noise on the hemispherical surface for the range of stiffnesses shown in Figure 10 is entirely consistent with the distribution of sound pressure on the horizontal observer plane shown in Figure 3. The significant reduction in the maximum far-field BVI noise of approximately 7 dB for the stiffened rotor and 8 dB for the rigid rotor compared to that of the teetering configuration is also consistent with the distribution of sound pressure on the horizontal observer plane described earlier.

Interpretation of the far-field noise for the high speed case requires more care since Doppler amplification causes the contribution from thickness noise to become more significant as flight speed is increased. This is shown clearly in Figure 12 where, at high speed ($\mu = 0.24$), a significant difference between the total BVI noise and the component due to loading is apparent. At low speed ($\mu = 0.12$), however, there is no notable difference between the total BVI noise and the loading noise. Indeed, when the thickness component of noise is included in the analysis at high speed, the point of maximum BVI sound pressure level lies within the plane of the rotor. Figure 11 hence shows only the loading component of the BVI sound pressure level on the hemispherical surface in order to allow an unbiased representation of the BVI noise characteristics in the far-field. The change in the directivity of the BVI noise towards the front left of the rotor is consistent with the change in the directivity observed on the horizontal observer plane as shown in Figure 3.

The maximum overall sound pressure level on the hemispherical surface, at both $\mu = 0.12$ and $\mu = 0.24$, does not appear to be affected significantly by the introduction of stiffness into the rotor system (see Figure 12). This suggests that, despite the significant reduction in the BVI noise that is achieved by increasing the hub stiffness, the sig-

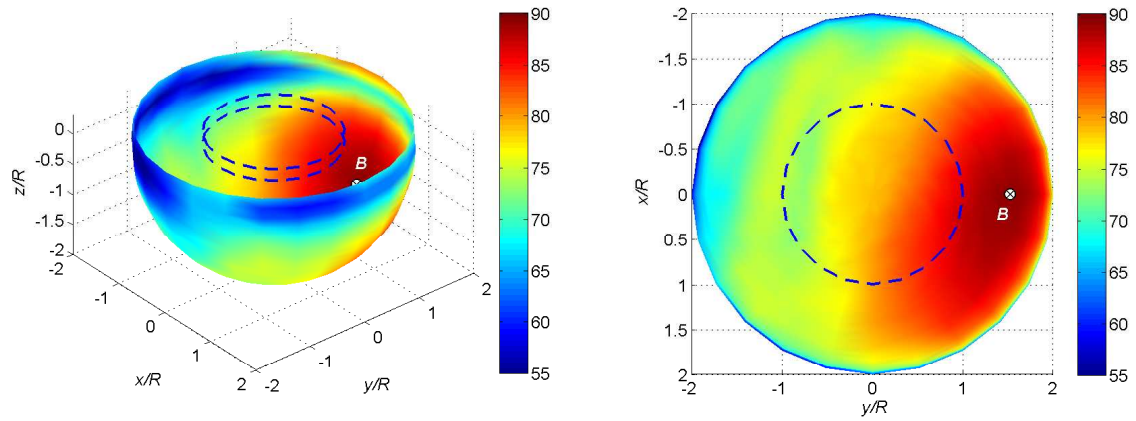

(a) Teetering rotor (sound pressure at 'B' is 89.2 dB)

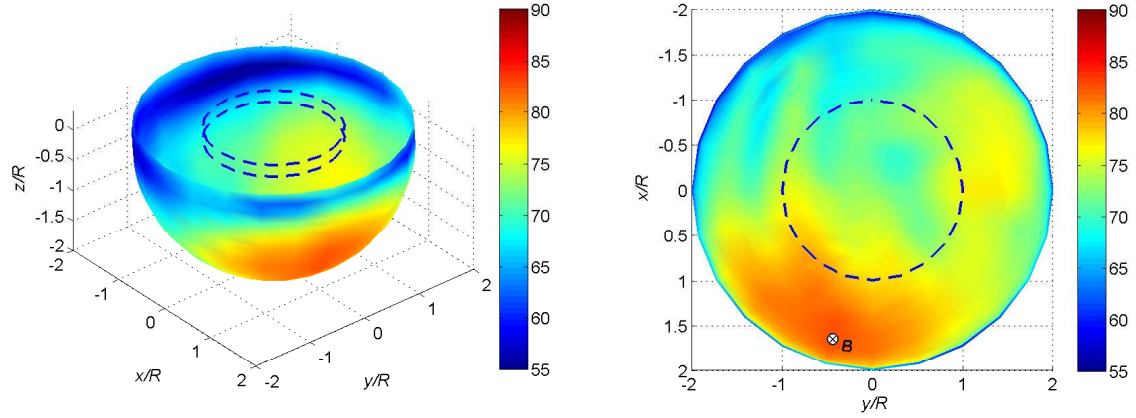

(b) Rotor stiffened to give first flapping frequency $\nu = 1.5$ (sound pressure at 'B' is 82.3 dB)

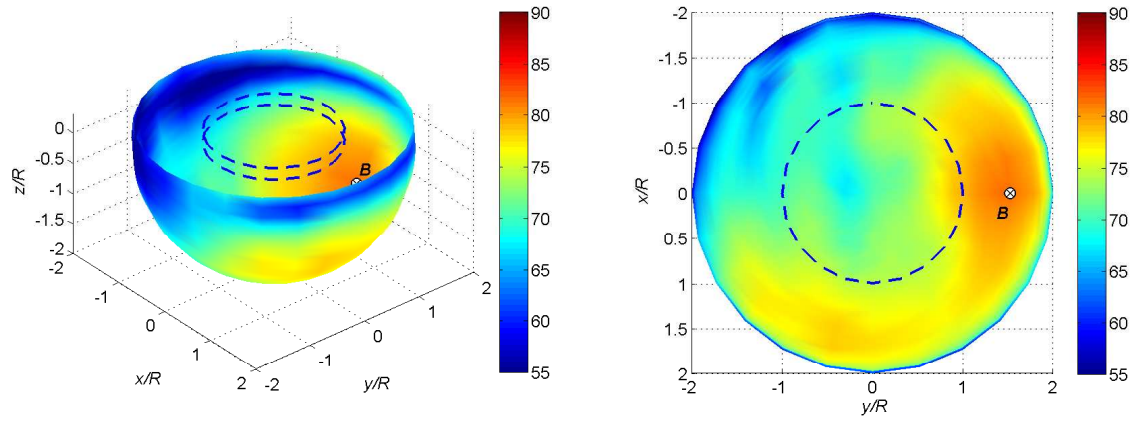

(c) Rigid rotor (sound pressure at 'B' is 81.3 dB)

Figure 10: *BVISPL in decibels on a hemispherical surface of radius* $2R$ *centred on the hub of the lower rotor. Advance ratio* $\mu = 0.12$. *(Left: isometric view. Right: top view.)*

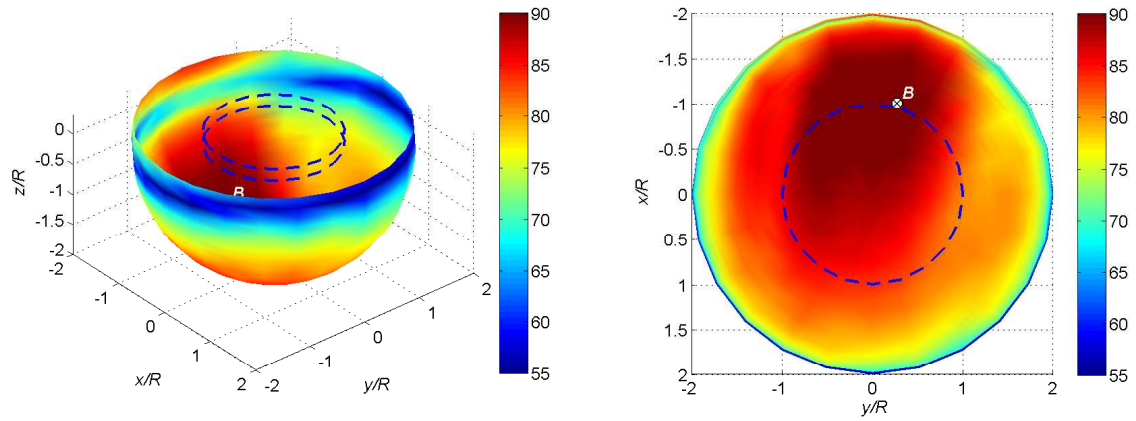

(a) Teetering rotor (sound pressure at 'B' is 91.0 dB)

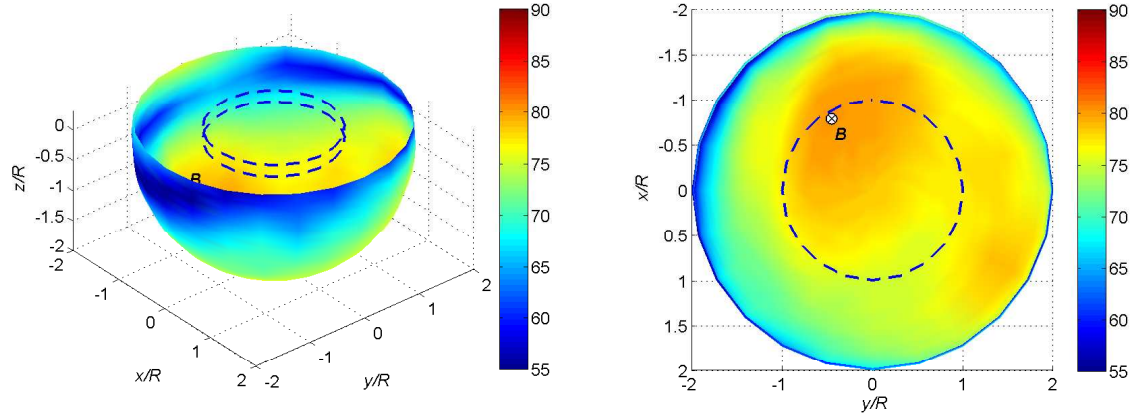

(b) Rotor stiffened to give first flapping frequency $\nu = 1.5$ (sound pressure at 'B' is 80.2 dB)

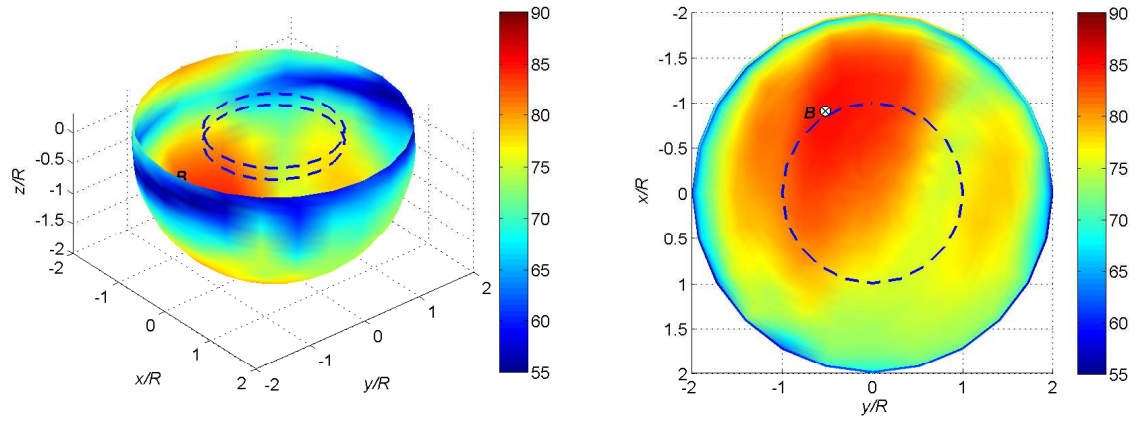

(c) Rigid rotor (sound pressure at 'B' is 85.0 dB)

Figure 11: *Loading noise BVISPL in decibels on a hemispherical surface of radius 2R centred on the hub of the lower rotor. Advance ratio* $\mu = 0.24$. *(Left: isometric view. Right: top view.)*

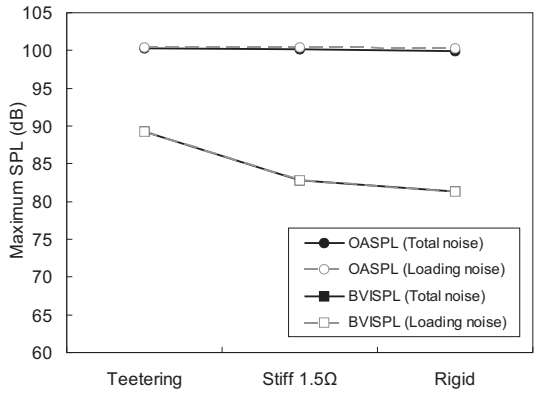

(a) $\mu = 0.12$ (Note that in Ref. 12, the loading OASPL and BVISPL noise for an equivalent single rotor were found to be 92.9 dB and 72.7 dB respectively.)

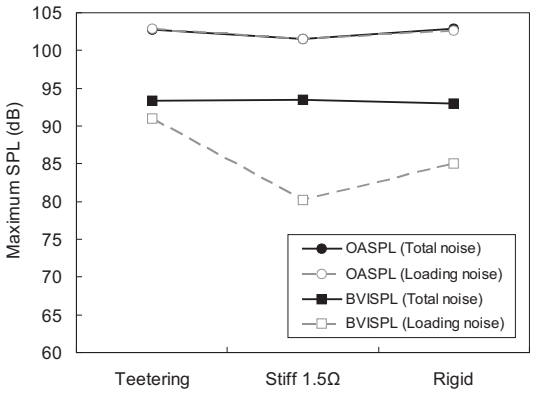

(b) $\mu = 0.24$ (Note that in Ref. 12, the loading OASPL and BVISPL noise for an equivalent single rotor were found to be 94.3 dB and 64.4 dB respectively.)

Figure 12: *Comparison of maximum OASPL and BVISPL (of total noise and loading noise only) in decibels on a hemispherical surface of radius* $2R$ *centred on the hub of the lower rotor.*

nificance of the low harmonic noise increases also, thus offsetting to a certain extent the benefits of stiffening in terms of overall sound pressure level. The results presented above suggest, however, that the intensity and directivity of the noise that is produced by the inter-rotor BVIs could quite feasibly be altered by careful partition of the loads between the upper and lower rotors of the stiffened coaxial system. Furthermore, individual rotor control in the context of stiffened coaxial systems, for example by using differential cyclic pitch inputs as described in the following section of the paper, is known to offer significant flexibility in controlling the load distribution on the rotors and may potentially also be exploited to alter the low harmonic acoustic characteristics of the coaxial system.

Effect of Lateral Lift Offset

The results of the computational results presented above suggest that a marked reduction in the BVI noise that is produced by the coaxial rotor might result from the introduction of significant flapwise stiffness into the system. This reduction appears to be a direct result of the weakening of the interaction between the lower rotor and the wake of the upper rotor wherein the principal inter-rotor BVI that is responsible for a significant proportion of the acoustic radiation from the system is reduced in its severity. This weakening occurs principally because the tip vortex that is trailed from the retreating blade of the upper rotor is reduced in strength due to the offloading of this part of the rotor that results from the introduction of flapwise stiffness into the system. The marked reduction of the intensity of the BVI noise that results from this change in the loading distribution on the rotor leads to the speculation that it might be possible to modify further the acoustic characteristics of the stiffened coaxial rotor by exacerbating the lateral asymmetry of the loading distribution on the upper rotor. In a stiffened coaxial rotor system, the lateral distribution of loading on the rotors can be modified readily, while still maintining overall lateral trim, by applying a differential cyclic pitch input to the upper and lower rotors of the system.

The lift offset is defined as the lateral distance between the centre of the rotor and the point of application of the lift vector of the rotor. Hence, for a rotor producing a rolling moment, C_{Mx}, and overall thrust, C_T, the lift offset, y_{LOS}, measured as a fraction of the rotor radius, R, is simply

$$y_{LOS} = C_{Mx}/C_T \,. \tag{1}$$

The effect on the acoustic properties of the stiffened coaxial rotor of changing the lateral distribution of loading on the rotors has been investigated. The effective lateral lift offset of the stiffened coaxial system has been controlled by applying independent lateral cyclic control inputs to the upper and lower rotors of the system in order to modify the rolling moment generated by each rotor whilst still maintaining an overall trim condition of zero net rolling moment. The results presented henceforth are obtained by altering the lift offset by approximately 20% to either side of the baseline value that was obtained when using coupled cyclic control to both the upper and the lower rotors. The baseline values of the lift offset, as measured from the simulations presented in the previous section, are found to be dependent on the flight speed. For both the stiffened rotor and the rigid rotor, the baseline lift offsets are measured as $y_{LOS} = 0.14R$ and $0.29R$ at advance ratios of $\mu = 0.12$ and 0.24 respectively.

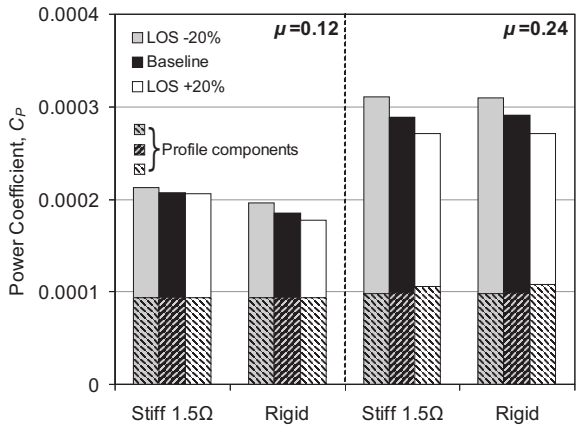

Figure 13: *The effect of lift offset on the power consumption of the stiffened coaxial rotor and the rigid coaxial rotor in forward flight.*

All other aspects of flight condition and trim are maintained exactly as those of the simulations presented in the previous section.

Figure 13 shows the influence of lift offset on the power consumed by the stiffened and the rigid coaxial systems. At both high and low forward speed, the power consumed by the rotors is seen to reduce as the imposed lift offset is increased. The results presented in this figure are consistent with previously published work [1] that has suggested that increasing the lift offset might improve the efficiency of the stiffened coaxial rotor. The reduction in power is found to be greater at the higher advance ratio where a reduction of approximately 8% is predicted if the lift offset is increased by 20%. It is interesting to note, though, that the reduction in the overall power consumption observed in this figure originates almost exclusively from a reduction in the induced power consumption of the rotor. In fact, the VTM suggests that the profile component of power should increase somewhat as the lift offset is increased, particularly at higher forward flight speeds.

Beyond illustrating the favourable effects on rotor performance of increasing the lift offset, further analysis of cause and effect will be avoided here since such a discussion would digress too far from the acoustic focus of this paper. The results presented in this section do raise the question, however, as to whether the imposition of significant lift offset might have the same positive effect on the acoustic characteristics of the stiffened coaxial system as it appears to have on its performance. This aspect is discussed in detail in the next section of this paper.

Acoustic Characteristics

Figure 14 summarises the influence of lift offset on the maximum sound pressure level that is observed on the horizontal plane located $1R$ below the hub of the lower rotor. At low advance ratio ($\mu = 0.12$), the maximum sound pressure level that occurs on the observer plane appears to be relatively insensitive to changes in the lift offset. At high advance ratio ($\mu = 0.24$), however, a notable sensitivity of the maximum sound pressure levels to the imposed lift offset is observed. It is interesting to note though the opposing trends in the overall sound pressure level (OASPL), which increases with increased lift offset, and the BVI sound pressure level (BVISPL), which decreases with increased lift offset. This appears to be due to a secondary effect which is discussed later.

The major source of noise in the mid-frequency range, as identified in the previous section of the paper, is the inter-rotor BVI that occurs on the advancing side of the lower rotor. Figure 15 shows the changes in the lateral distribution of blade loading on the upper and lower rotors of the coaxial system that result from altering the lift offset. It is apparent from the figure that, as the effective lift is offset further outboard towards the tip of the advancing side of the disc, the lateral distribution of loading on the rotor is modified such that the loading peak on the advancing side is increased in amplitude. The tip loading on the retreating side, on the other hand, is shown to be reduced as a result of this change in the lift offset. The tip vortex trailed from the retreating blade of the upper rotor is thus reduced in strength (as is the equivalent vortex trailed from the retreating blade on the lower rotor). Bearing in mind that the vortex that is associated with the principal sound-generating interaction is trailed from the tip of the retreating blade on the upper rotor of the system, this chain of cause and effect conspires to ameliorate the loading component of the BVI noise by weakening the principal inter-rotor BVI when the lift offset is increased.

Figure 16 shows the effect of lift offset on the acoustic source density on the lower rotor and reveals that the acoustic source at the location of maximum sound pressure level is concentrated at the location of the principal BVI. It is also evident in this figure that the region of high acoustic source density on the lower rotor is increasingly confined to the BVI location as the lift offset is reduced.

Figure 14 shows that the overall sound pressure level (OASPL) also increases as the imposed lift offset on the system is increased. Figure 17 shows the effect of lift offset on the time history of the acoustic pressure observed at the point of maximum sound pressure on the observer plane $1R$ below the rigid coaxial rotor at advance ratio $\mu = 0.24$. The signal

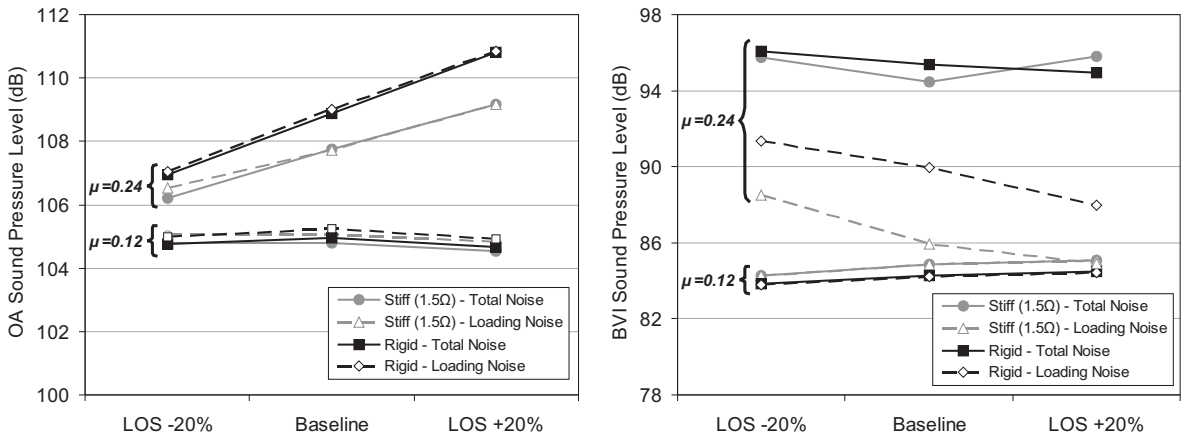

(a) OASPL (b) BVISPL

Figure 14: *Effect of lift offset on maximum SPL as observed on a horizontal plane* $1R$ *below the hub of the lower rotor.*

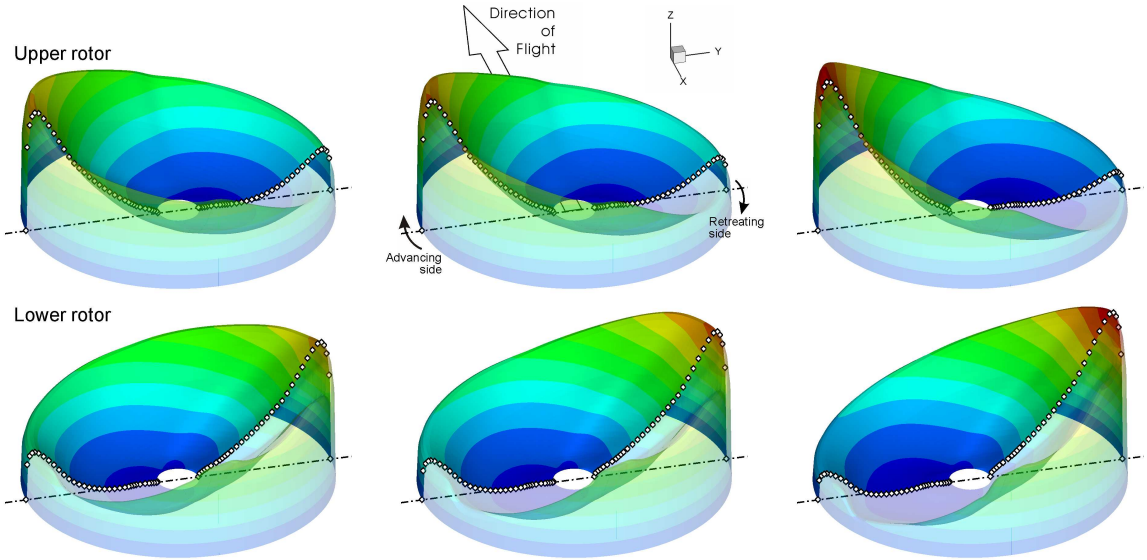

(a) LOS -20% (b) Baseline (c) LOS +20%

Figure 15: *Effect of controlling the lift offset on the azimuthal variation of blade loading for the rigid coaxial rotor at advance ratio* $\mu = 0.24$*. The distribution is sectioned to expose more clearly the effect of lift offset on the lateral distribution of loading on the upper and lower rotors.*

plotted in this figure has been filtered to contain only the first ten harmonics of the rotor rotational frequency. It is clear from this figure that the peak to peak variation in the low harmonic component of the acoustic pressure signal is increased by increasing the lift offset and vice versa. This observation could perhaps have been inferred from Figure 15 where the maximum blade loading was shown to increase as a larger lateral lift offset is imposed on the rotors.

As was done in slightly different context earlier in this paper, the effect of lift offset on the radiation of noise to the far-field can be estimated by calculating the acoustic pressure on a hemisphere of radius $2R$ centred at the hub of the lower rotor. The effect of lift offset on the maximum sound pressure levels observed on this hemispherical surface is summarised in Figure 18. A striking similarity in the trend shown in this figure to that observed on the horizontal plane $1R$ below the rotor (as shown in Figure 14) is clearly apparent. This is a strong indication that the influence of lift offset on the noise produced by the rotor has the same physical origins as the effect of stiffness as described earlier

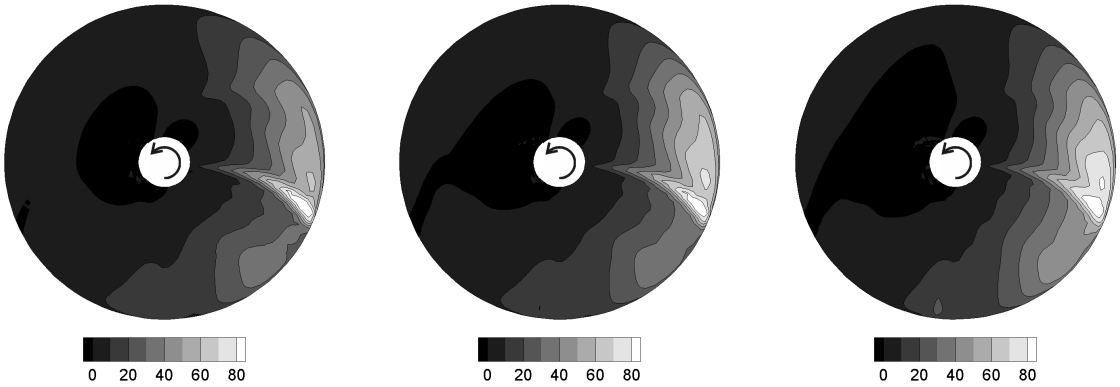

(a) LOS -20% (b) Baseline (c) LOS +20%

Figure 16: *Acoustic source density (loading noise, Pa/m^2) on the lower rotor of the rigid coaxial system as evaluated at the BVI hot spot at advance ratio $\mu = 0.24$.*

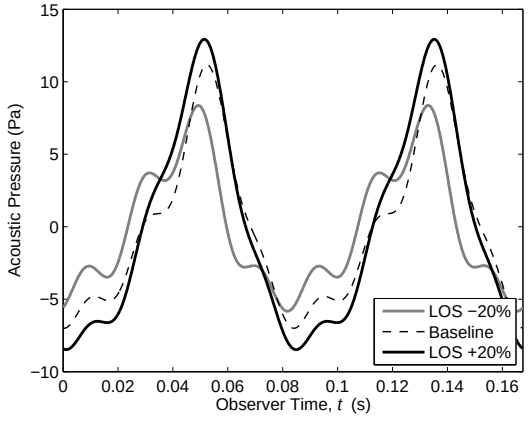

Figure 17: *Time history of acoustic pressure over one revolution of the rigid coaxial rotor, as observed at the BVI hot spot at advance ratio $\mu = 0.24$. Acoustic signal filtered to include only the first 10 harmonics of the rotor rotational frequency.*

in the paper.

The greatest sensitivity to the imposed lift offset, as shown in Figure 18, is seen in the loading component of the BVI noise at high advance ratio. Furthermore, it is only at this advance ratio that a significant disparity between the total noise and loading noise is observed. This is because the effect of the thickness component of noise becomes significant at high speeds. The thickness noise, however, is propagated primarily within the plane of the rotor. The loading noise is directed primarily out of the plane of the rotor, and hence has greater significance for the overall acoustic signature of the rotor system. Figure 18 thus suggests that an effective reduction in BVI noise of about 2 dB is achievable, at least for the present rotor configuration, by increasing the lift offset by 20%.

On the other hand, the maximum BVI noise level for the stiffened coaxial rotor increases, though only by about 0.5 dB, when the lift offset is increased by 20% at advance ratio $\mu = 0.24$. This rise in the BVI noise level is somewhat unexpected considering that an increase in lift offset acts to weaken the inter-rotor BVI that is primarily responsible for the acoustic radiation of the system, as described earlier. Figure 19, which shows the effect of lift offset on the distribution of loading noise within the BVI frequency range, reveals the hemispherical observer surface to contain two acoustic hot spots (marked 'B' and 'B2'), however. Figure 20, showing the time history of acoustic pressure at the hot spots marked 'B' together with the density of acoustic sources on the lower rotor for the two cases presented in Figure 19, reveals that the acoustic signatures that are associated with the two different hot spots are significantly different in character and thus most likely are caused by distinctly different mechanisms. The highly impulsive nature of the pressure peaks shown in Figure 20(a) is indicative of their origin in an intense BVI within the rotor system whereas the much less impulsive nature of the peaks shown in Figure 20(b), although similar in amplitude to those of Figure 20(a), suggests that their origin is to be found in a BVI of lesser intensity. Indeed, the former, more intense interaction is caused by the direct, parallel impact of tip vortex on blade that is associated with the primary BVI on the advancing side of the lower rotor. Closer investigation reveals the latter, less intense interaction to be induced by a slightly earlier interaction between the same blade and the vortex sheet that is generated inboard of the tip vortex that is associated with the primary BVI. These observations can be confirmed as follows.

In Figure 20(a), the locus of sources, corresponding to the observer time at which the largest peak in

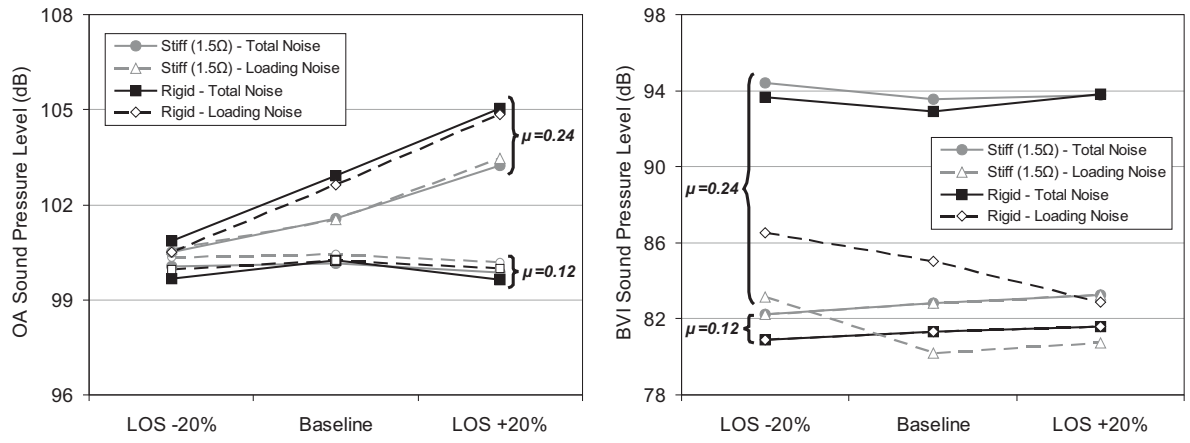

(a) OASPL (b) BVISPL

Figure 18: *Effect of lift offset on maximum SPL as observed on a hemispherical observer surface of radius* $2R$ *centred on the hub of the lower rotor.*

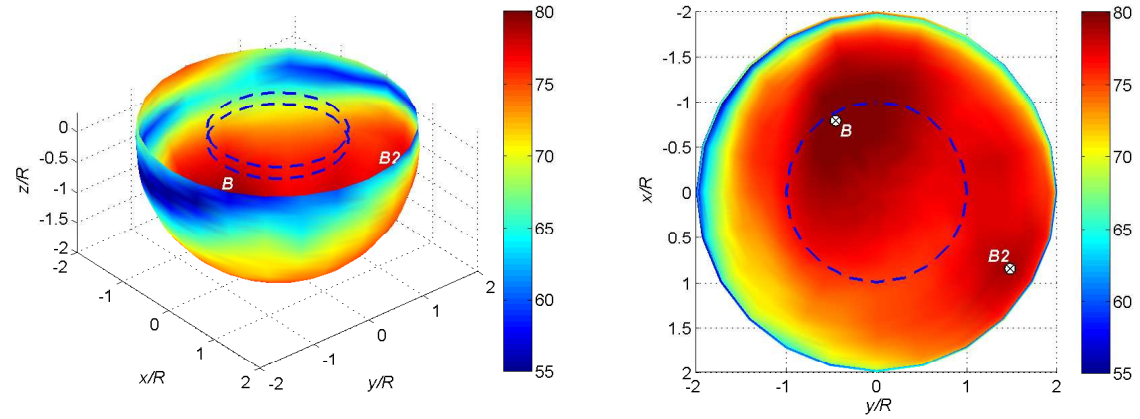

(a) Baseline (sound pressure at 'B' is 80.2 dB and at 'B2' is 78.9 dB)

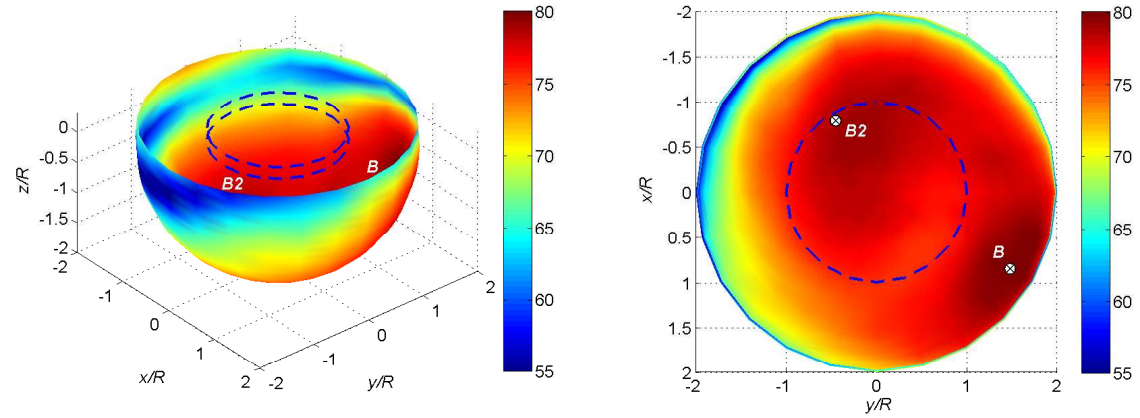

(b) LOS +20% (sound pressure at 'B2' is 78.7 dB and at 'B' is 80.7 dB)

Figure 19: *Loading noise BVISPL (in decibels) on a hemispherical surface of radius* $2R$ *centred on the hub of the lower rotor. Coaxial system stiffened to* $\nu = 1.5$ *with different lift offsets at advance ratio* $\mu = 0.24$*. (Left: isometric view. Right: top view.)*

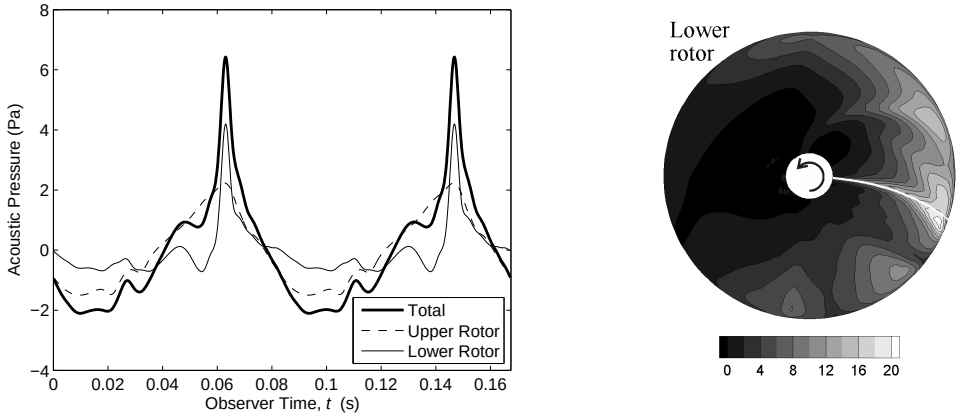

(a) Baseline (locus of sources on right corresponds to observer time $t = 0.063\,\mathrm{s}$)

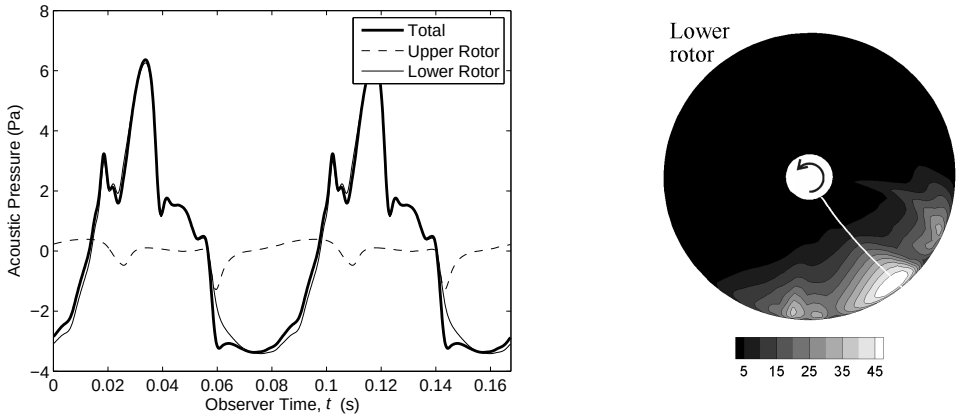

(b) LOS +20% (locus of sources on right corresponds to observer time $t = 0.034\,\mathrm{s}$)

Figure 20: *Time history of acoustic pressure over one rotor revolution (left) and the acoustic source density (loading noise, Pa/m^2) on the lower rotor of the coaxial system stiffened to $\nu = 1.5$ (right) for different lift offsets at advance ratio $\mu = 0.24$. Both plots as evaluated at the BVI hot spot marked 'B' in Figure 19.*

the acoustic pressure occurs, is indicated as a white line on the plot of the acoustic source density. The resulting locus for the baseline rotor is very similar to that shown in Figure 8 and confirms that the parallel inter-rotor BVI shown in Figure 9 is the principal source of noise at the hot spot marked 'B' in Figure 19(a).

In contrast, the broad range of azimuth that is occupied by the region of high source density shown in Figure 20(b), for the case of increased lift offset, is consistent with the non-impulsive character of the peak observed in the time history contained in the same figure. The locus of sources, corresponding to the observer time at which this peak occurs, is positioned at an azimuth of approximately $\psi = 40°$ on the lower rotor of the coaxial system. Figure 21 shows the rotor and its wake at the corresponding instant and reveals the blade of the lower rotor to be interacting closely with the inboard vortex sheet that is generated behind one of the blades of the upper rotor. The weakness of this vortex sheet compared to its associated tip vortex and the almost tangential orientation of the sheet to the trajectory of the blade results in a weaker, more prolonged interaction that is consistent with the acoustic source distribution that is shown in Figure 20(b).

As the lift offset is increased, the strength of the primary inter-rotor BVI is reduced to such an extent that this particular interaction is no longer the most significant contributor to the maximum BVI sound pressure level that is observed on the hemispherical observer surface. Indeed, Figure 20 shows that although the two hot spots (marked 'B' and 'B2') are located at approximately the same position regardless of lift offset, the hot spot associated with the parallel interaction ('B' in Figure 19(a)) is the more intense in the baseline case whereas the hot spot associated with the sheet interaction ('B' in Figure 19(b)) is the more intense when the lift offset is increased.

These observations show that it might indeed be

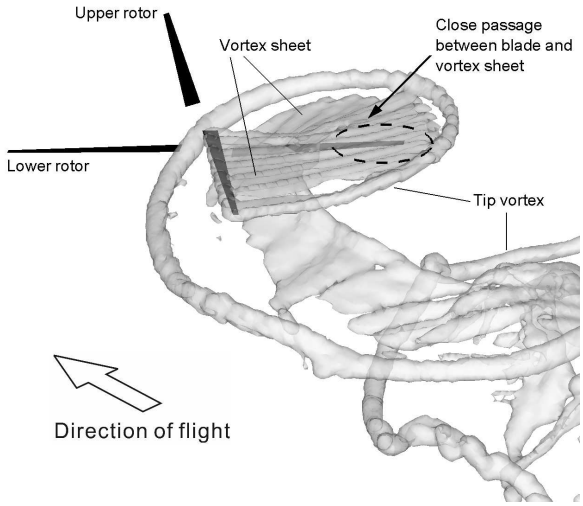

Figure 21: *Close passage interaction between a blade of the lower rotor and the vortex sheet shed by a blade of the upper rotor. Stiffened system at advance ratio* $\mu = 0.12$.

possible to exploit lift offset to reduce the acoustic signature of the stiffened coaxial rotor system, but also caution that the benefits of such a strategy may be limited by the emergence of other, perhaps unforseen but nonetheless inherent interactions within the system as the dominant contributor to the acoustic characteristics of the system.

Conclusions

The aeroacoustic characteristics of a coaxial rotor with significant flapwise stiffness are computed using the Farassat-1A formulation of the Ffowcs Williams-Hawkings equation coupled to the Vorticity Transport Model and compared to those of a conventionally articulated coaxial rotor both in low speed and in high speed forward flight.

The most prominent source of impulsive noise in a conventionally articulated coaxial rotor system is a strong, parallel interaction which occurs between the blades on the advancing side of the lower rotor and the tip vortices that are generated by the blades on the retreating side of the upper rotor.

Introduction of significant flapwise stiffness yields a marked reduction in the BVI noise that is produced by the coaxial system. This is a direct consequence of the weakening of the principal inter-rotor BVI as a result of the broad redistribution in lateral loading on the upper rotor that accompanies the introduction of flapwise stiffness into the system. This weakening occurs simply because the tip vortex that is associated with the primary interaction is reduced in strength as the blades on the retreating side of the upper rotor are offloaded. The introduction of significant flapwise stiffness into the rotor system that was studied yields a reduction in maximum BVI sound pressure level, as measured on a hemispherical surface located two rotor radii from the rotor hub, of approximately 7–8 dB at advance ratio $\mu = 0.12$, and 6–11 dB at advance ratio $\mu = 0.24$.

The spanwise distribution of loading (i.e. the lift offset) on the rotors of a stiffened coaxial system can be modified by differential cyclic pitch input. It is shown that increasing the lift offset produces a notable reduction in both the power consumed by the rotor and also the BVI noise, particularly at higher advance ratio. Simulations of a rigid coaxial system suggest that a reduction of about 2.1 dB in the BVI noise and 6.8% in power consumption might result from increasing the lift offset by 20% from the nominal baseline value at advance ratio $\mu = 0.24$. The effectiveness of lift offset in reducing the acoustic signature of the rotor at high forward speed is constrained, however, because an interaction between the blades of the lower rotor and the sheets of vorticity that are trailed from the inboard parts of the blade of the upper rotor replaces the parallel BVI on the advancing side of the lower rotor as the dominant source of noise within the system.

The results presented in this paper thus show that it might indeed be possible to exploit lift offset to reduce the acoustic signature of the stiffened coaxial rotor system, but also caution that the benefits of such a strategy may be limited by the emergence of other, perhaps unforeseen but nonetheless inherent interactions within the system as the dominant contributor to the acoustic characteristics of the system.

It should also be borne in mind that, while the assumption that the dynamics of the stiffened coaxial system can be characterised using a flap spring in conjunction with otherwise rigid rotor blades might yield a reasonable global representation of the overall aeroacoustic characteristics of the relatively generic coaxial rotor modelled in this study, direct application of the results presented here to real helicopter configurations may have to await the incorporation of a structural dynamic model to account more fully and accurately for the flexure of the blades.

References

[1]Bagai, A., "Aerodynamic Design of the Sikorsky X2 Technology Demonstrator^{TM} Main Rotor Blade," American Helicopter Society 64th Annual Forum, Montréal, Canada, 29 April–1 May 2008.

[2]Burgess, R.K., "The ABC^{TM}Rotor — A His-

torical Perspective," American Helicopter Society 60th Annual Forum Proceedings, Baltimore, MD, 7–10 June 2004.

[3]Cheney, M.C. Jr., "The ABC Helicopter," *Journal of the American Helicopter Society*, Vol. 14, No. 4, October 1969, pp. 10–19.

[4]Paglino, V.M., "Forward Flight Performance of a Coaxial Rigid Rotor," American Helicopter Society 27th Annual National V/STOL Forum, Washington, D.C., May 1971.

[5]Ruddell, A.J., "Advancing Blade Concept (ABC™) Development," American Helicopter Society 32nd Annual National V/STOL Forum, Washington, D.C., 10–12 May 1976.

[6]Kim, H.W., Brown, R.E., "Coaxial Rotor Performance and Wake Dynamics in Steady and Manoeuvring Flight," American Helicopter Society 62nd Annual Forum Proceedings, Phoenix, AZ, 9–10 May 2006.

[7]Kim, H.W., Brown, R.E., "Impact of Trim Strategy and Rotor Stiffness on Coaxial Rotor Performance," 1st AHS/KSASS International Forum on Rotorcraft Multidisciplinary Technology, Seoul, Korea, 15–17 October 2007.

[8]Leishman, J.G., *Principles of Helicopter Aerodynamics, Second Edition*, Cambridge University Press, Cambridge, UK, 2006.

[9]Anikin, V.A., "Aerodynamic Feature of a Coaxial Rotor Helicopter," Paper No. 66, 17th European Rotorcraft Forum, Berlin, Germany, 24–27 September 1991, pp. 533–551.

[10]Peterson, R.L., Mosher, M., "Acoustic Measurements of a Full-Scale, Coaxial, Hingeless Rotor Helicopter," NASA TM-84349, June 1983.

[11]Boyd, D.D. Jr., Burley, C.L., Conner, D.A., "Acoustic Predictions of Manned and Unmanned Rotorcraft Using the Comprehensive Analytical Rotorcraft Model for Acoustics (CARMA) Code System," American Helicopter Society International Specialists' Meeting on Unmanned Rotorcraft, Phoenix, AZ, 18–20 January 2005.

[12]Kim, H.W., Duraisamy, K., Brown, R.E., "Aeroacoustics of a Coaxial Rotor in Level Flight," American Helicopter Society 64th Annual Forum Proceedings, Montréal, Canada, 29 April–1 May 2008.

[13]Brown, R.E., "Rotor Wake Modeling for Flight Dynamic Simulation of Helicopters," *AIAA Journal*, Vol. 38, No. 1, January 2000, pp. 57–63.

[14]Brown, R.E., Line, A.J., "Efficient High-Resolution Wake Modeling Using the Vorticity Transport Equation," *AIAA Journal*, Vol. 43, No. 7, April 2005, pp. 1434–1443.

[15]Farassat, F., Succi, G.P., "A Review of Propeller Discrete Frequency Noise Prediction Technology with Emphasis on Two Current Methods for Time Domain Calculations," *Journal of Sound and Vibration*, Vol. 71, No. 3, 1980, pp. 399–419.

[16]Schmitz, F., Yu, Y., "Theoretical Modeling of High-Speed Helicopter Impulsive Noise," *Journal of the American Helicopter Society*, Vol.23, No.1, 1979.

[17]van der Wall, B.G., Junker, B., Burley, C.L., Brooks, T.F., Yu, Y.H., Tung, C., Raffel, M., Richard, H., Wagner, W., Mercker, E., Pengel, K., Holthusen, H., Beaumier, P., Delrieux, Y., "The HART II Test in the LLF of the DNW—a Major Step towards Rotor Wake Understanding," 28th European Rotorcraft Forum, Bristol, UK, 17–20 September 2002.

[18]Kelly, M.E., Duraisamy, K., Brown, R.E., "Blade Vortex Interaction and Airload Prediction using the Vorticity Transport Model," American Helicopter Society Specialists' Conference on Aeromechanics, San Francisco, CA, 23–25 January 2008.

[19]Harrington, R.D., "Full-Scale-Tunnel Investigation of the Static-Thrust Performance of a Coaxial Helicopter Rotor," NACA TN-2318, March 1951.

[20]Dingeldein, R.C., "Wind-Tunnel Studies of the Performance of Multirotor Configurations," NACA TN-3236, August 1954.

[21]Kitaplioglu, C., Caradonna, F.X., "A Study of Blade-Vortex Interaction Aeroacoustics Utilizing an Independently Generated Vortex," AGARD Fluid Dynamics Panel Symposium on Aerodynamics and Aeroacoustics of Rotorcraft, Berlin, 10–14 October 1994.

[22]Leishman, J.G., "Sound Directivity generated by Helicopter Rotors using Wave Tracing Concepts," *Journal of Sound and Vibration*, Vol. 221, No. 3, 1999, pp. 415–441.